New insight into bacterial iron competition: A-to-I editing in ferric entero bactin uptake

Wenhan Nie [1*], Sai Wang [1*], Qin Xu [2], Peihong Wang [1], Yan Wu [1], Rui He [3], Ayizekeranmu Yiming [1], Jingling Liang [1], Iftikhar Ahmad [1,5], Luoyi Fu [1], Longbiao Guo [4], Junhua Yuan [3], Bo Zhu [1$], Gongyou Chen [1$]

[1] Key Laboratory of Urban Agriculture by Ministry of Agriculture of China, School of Agriculture and Biology, Shanghai Jiao Tong University, Shanghai, China

[2] State Key Laboratory of Microbial Metabolism, and SJTU-Yale Joint Center for Biostatistics and Data Science, School of Life Sciences and Biotechnology, Shanghai Jiao Tong University, Shanghai 200240, China

[3] Hefei National Laboratory for Physical Sciences at the Microscale and Department of Physics, University of Science and Technology of China, Hefei, Anhui, China

[4] State Key Lab for Rice Biology, China National Rice Research Institute, Hangzhou 310006, PR China

[5]Department of Environmental Sciences, COMSATS University Islamabad, Vehari-Campus, Vehari-61100, Pakistan

[*] Contribute equally

[$] To whom correspondence should be addressed

Contact: gyouchen@sjtu.edu.cn or bzhu1981@sjtu.edu.cn

Running Title: A-to-I editing in iron metabolism

ABSTRACT

Iron is an essential element for growth and survival of pathogenic bacteria. However, how these bacteria sense and respond to iron starvation or excess is still not fully understood. Here, we show that *xfeA* (a homolog of *fepA*) in *Xanthomonas oryzae*, can sense the extra-cytoplasmic iron concentration and change the 3D structure of ligand channel domain by A-to-I RNA editing. The percentage of A-to-I RNA editing was increased to 76.87% under iron-starvation, facilitating iron to pass through the XfeA channel without any interference to the strongest Iron(III)–siderophore $[Fe\text{-}(Ent)]^{3-}$. However, under high iron concentration, the percentage of A-to-I editing to *xfeA* was reduced, thereby restricting the Fe-Ent to pass iron through the channel of XfeA. The variations in concentration of Fe-Ent was sensed by methyl-accepting chemotaxis proteins (MCPs) at cytoplasmic membrane, which influences the expression of a number of chemotaxis related genes. This regulation drives the bacteria to move further towards the iron-rich direction. Overall, our results revealed a new signaling mechanism that bacterial iron sense and homeostasis are modulated through A-to-I RNA editing.

IMPORTANCE

A-to-I RNA editing, which is catalyzed by the adenosine deaminase, acts on RNA family of enzymes, is one of the most prevalent type of post-transcriptional modification in metazoans. However, the research of A-to-I editing in bacteria is limited and the importance of this editing is still underestimated. In this study, we found that bacteria may use A-to-I editing (*xfeA*, a homolog of *fepA*) as an alternative

strategy in iron metabolic uptake, as the editing event level can precisely regulate the RNA and the protein sequence within relatively short physiological time scales comparing with the traditional switch “on” and “off” regulation. To best of our knowledge, it is a new identified inching-switch-like mechanism by which pathogens may absorb iron better in order to compete with the hosts.

INTRODUCTION

Iron is one of the most abundant element in the Earth's crust and virtually essential for all forms of life, including bacteria during all aspect of cellular processes such as energy generation, respiration, photosynthesis, DNA replication to oxygen transport and protection against various stresses (1, 2). Bacterial pathogens must acquire iron within their hosts in order to survive and replicate. The competition of iron for pathogenic bacteria is extremely important because they invade the host plants or animals where iron is limited, the termed known as nutritional immunity (3). However, the hosts retain iron and other nutrients by sequestration with various proteins or small-molecular chemicals (4, 5). To compete for iron acquisition, bacteria developed very efficient iron (usually ferric Fe^{3+}) uptake mechanisms based on high-affinity iron-carriers, named siderophores (6), of which, enterobactin (Fe-Ent) is one of the strongest iron chelator, which is produced and secreted by many pathogenic bacteria (7).

Many Gram-negative bacteria including model plant pathogen *Xanthomonas oryzae*, can produce and take up this siderophore to scavenge iron (8). Generally, this

molecule is first synthesized within the bacterial cell and secreted through the cell membranes to capture Fe(III) from the environment. The resulting Fe(III)-enterobactin complex (Fe-Ent) is recognized at the bacterial cell surface by highly selective outer-membrane TonB-dependent receptors (TBDR) and actively transported into the periplasm (9). FepA is the most well characterized receptor in previous study. In periplasm, Fe-Ent is sequestered by the periplasmic binding protein (PBP), such as FepB, which transfers Fe-Ent to inner membrane transporter for further transport into the cytoplasm (6). Once there, Fe-Ent is hydrolyzed to release Fe(III) and convert to Fe^{2+} for further usage in the cell (10). Interestingly, we recently found that A-to-I editing event on the mRNA of *fliC* can enhance the Fe^{3+} uptake ability and thus, increase the biomass *in vivo* and enhance the virulence (11). Post-transcriptional A-to-I editing has been proved to be important in eukaryote however, it was recently reported in bacteria (12) and barely known of the biological function. Since the A-to-I RNA editing in K^+ channel's pore of octopus has been reported that could alter the channel open state to respond to the extreme cold environment (13), this raises the possibility that bacteria may also use the similar mechanism to regulate the iron uptake.

In this study, our objectives were to identify the biological function of A-to-I RNA editing event (T408A, threonine to alanine in the 408th amino acid) occurred in the *xoc_3486* (*Xanthomonas fepA* homolog, named *xfeA*) that may enhance the bacterial iron uptake capacity and the tolerance to iron depleted conditions, and to explore the occurrence conditions of the T408A editing event and demonstrate its

significance in bacterial chemotaxis and virulence.

RESULTS

The T408A editing level in *xoc_3486* (*xfeA*) depend on the environmental iron concentration

Previously, we have reported that the A-to-I RNA editing event occurred in *xfeA*, causing change in an amino acid from threonine to alanine at residue 408 (11). Here, we have analyzed potential editing events in cDNA samples from BLS256 WT in the presence of 2, 2'-dipyridyl (DP) and $FeCl_3$ as iron chelator and supplements, respectively (Fig. 1a). The results suggest that T408A editing level changed depending on the environmental iron concentration, generally the rate of A-to-I RNA editing rise with the depletion of environmental iron concentration. Specifically, in the presence of NB medium only, 21.27% of WT transcriptional samples showed editing events; however, hardly any editing event was detected in the samples of NB plus 100μM $FeCl_3$. In the samples of iron depletion, 37.39%, 76.87% and 78.03% of the cDNA samples exhibited the editing events in the presence of 50μM, 100μM and 150μM DP, respectively (Fig. 1a and 1b). To block the RNA editing, the synonymous mutation (ACG to ACA, red arrow) containing strain named $T408^{silent}$ was constructed, and hardly A-to-I RNA editing event was detected at this site (Fig. 1b and Fig. S5).

We analyzed the A-to-I RNA editing sites from RNA-seq data of T408A and $T408^{silent}$ strain growth in NB medium by AIMAP. Interestingly, 9 of 12 A-to-I editing sites were detected in both T408A and $T408^{silent}$ strain (Table S4, orange labeled) and the RNA editing patterns were generally coherent (Fig. S5). Besides, we checked the

A/G rate on *xfeA* T408A site from the reads of RNA-seq data, and the result suggested that the editing level of *xfeA* is 100% and 0% in T408A and T408^{silent} strain (Table S4, blue labeled and Fig. S5 red frame). Thus verifying the construction of T408^{silent} strain could block the A-to-I RNA editing of *xfeA* and highlighting the importance of the motif.

Interestingly, the editing event is independent on the *tadA* (tRNA-specific adenosine deaminase), in spite of both the TACG motif and the RNA secondary structure (in a loop) coincide with the enzyme recognized (12) (Fig. 1b and Fig. S2). In addition, no homologues of adenosine deaminase *rdrB* were found in *Xanthomonas oryzae* genome, which was recently identified by Gao (14) and named phage restriction by an adenosine deaminase acting on RNA (RADAR). Since the A-to-I RNA editing was blocked in T408^{silent} strain, we hypothesized that the *xfeA* T408A mutation was induced by iron deficiency and catalyzed by an (or several) unknown enzyme(s), as well as the recognition base on the motif.

T408A editing is predicted to impact the structure of XfeA

The XfeA protein is a homolog of FepA which is the ferric enterobactin (Fe-Ent) outer membrane receptor protein (15). Furthermore, FepA plays an important role of Fe-Ent entry which is the most important way of iron uptake in many gram negative bacteria (16, 17). Thus, it was hypothesized that the T408A editing event could change the efficiency of Fe-Ent entry, and thereby cause variations in the ability of iron uptake. To further investigate the impact of the T408A exchange, a three-dimensional homology model of XfeA was constructed based on the crystal

structure of a similar TBDR, PiuA from *A. baumannii* (PDB ID: 5FP1) (18). In this model, XfeA is composed with a 22-stranded transmembrane β-barrel surrounding a plug domain as other TBDRs (Fig. 2a). The mutated residue Thr408 is on the edge of the entrance of the β-barrel, with its side chain hydrogen-bonded with those of Glu416 and Gln453 (Fig. 2b in red circle). This local hydrogen bonding network may help to fix the flexible extracellular segment of 408-420, with the long side chains of the residues Arg418 and Arg419 pointing toward the entrance that may contribute to the binding of the ligands.

T408A mutants show increased tolerance to iron depleted stress

Since the T408A editing event was induced by iron depletion, we hypothesized that editing event may contribute in environmental iron deficiency. To further investigate, the growth curve of BLS256 WT, $T408^{silent}$ and the A-G point mutation containing strain named T408A were compared without and with the presence of 50μM, 100μM and 150μM DP in NB medium (Fig. 3 a-d). The strains grown in NB medium without or with 50μM DP showed similar growth patterns (Fig. 3a and 3b); however, lower growth rate of log phase and longer time of lag phase were observed in the WT and $T408^{silent}$ strains grown in NB supplemented with 100μM and 150μM DP (Fig. 3c and 3d). The T408A strains (fixed 100% editing level) in growth interfering level of DP showed enhanced tolerance, while WT (free to edit) showed a slightly higher tolerance to iron depletion when compared with $T408^{silent}$ (block editing). Notably, these results suggest that the level of T408A editing could help *Xoc* adapt to environmental iron deficiency.

T408A editing enhance the iron uptake ability

The intracellular concentration of total iron in the T408A, T408^{silent} and WT strains were quantified with inductively coupled plasma optical emission spectrometry (ICP-OES). In the NB medium plus 50μM DP, the iron accumulation in *Xoc* cells of T408A and WT strains significantly increased by 76.0% and 46.9%, respectively of the level in the T408^{silent} strain (Fig. 3e). In the NB medium, the iron concentration in the T408A and WT strains also increased by 175.3% and 110.1%, respectively to the levels in the T408^{silent} strain. Under iron-replete condition (NB+100μM $FeCl_3$), the iron content of T408A mutation also 145.6% higher than T408^{silent} while the level of WT still 23.6% higher than T408^{silent} (Fig. 3e). This may be related to the decline of the WT editing level in high iron concentration condition. The sufficient free iron leads the T408A strain showed a better iron uptake performance in iron supplement, and iron uptake of other pathways may lead the smaller difference between T408A and T408^{silent} strains in iron limitation. These results exhibit the importance of T408A RNA editing on *xfeA* for iron uptake.

Streptonigrin (SNG) is a drug that the iron is indispensable for its bacteriostatic activity and its toxic effect is proportional to the intracellular iron concentration (2, 19). To further characterize the relationship between T408A editing and iron uptake, resistance of *Xoc* strains to SNG was measured. In the presence of 1 μg/mL SNG, the survival rate of T408A was strongly lower (by 69.8%), whereas the WT was lower (by 23.2%) than T408^{silent}. Under the iron-depleted condition (NB plus 50μM DP), the survival rates of three stains were varying degrees of upward (Fig. 3f). Whereas the

ordering of strains survival rate was unaltered (T408A < WT < T408^{silent}). Taken together, these results supported the view that *xfeA* T408A editing event could help *Xoc* to take-up iron, especially it could increase the tolerance to iron depleted stress.

T408A editing upregulates genes related to chemotaxis pathway

The RNA-seq was used to compare the T408A and T408^{silent} strains to further investigate the change of *xfeA* T408A editing for *Xoc*. However, before comparing RNA-seq profiles of two strains, reproducibility was evaluated for two replicate experiments using pairwise linear correlation analysis. The correlation coefficients (*r*) between the two replicate experiments were 0.991 and 0.998, suggesting satisfactory reproducibility of RNA-seq data under the experimental conditions. Based on the cutoff as described in the M & M section, 138 differentially expressed genes were identified (Fig 4a, Table S3). The KEGG pathway enrichment analysis suggested only one pathway (Bacterial chemotaxis) was enriched in these DEGs (Table. S3). Interestingly, 21 of 24 chemotaxis pathway genes were up-regulated at least 1.5-fold (FDR < 0.01). Based on the annotations, 5 genes (*xoc_2278*, two-component system response regulatory protein, CheB; *xoc_2280*, chemotaxis protein methyltransferase 2, CheR; *xoc_2289*, *xoc_2291*, *xoc_2297*, methyl-accepting chemotaxis protein, MCP) were selected to verify with qRT-PCR. The result suggested that the expression level of chemotaxis pathway genes generally positive correlation with the environmental iron concentration, and the level of T408A are overall higher than T408^{silent} (Fig. 4b). Besides, the expression of *xfeA* was independent of environmental iron content (Fig. 4b and Fig. S1). The chemotaxis pathway diagram of *Xoc* (based on KEGG) was

constructed to visually exhibit the influence of T408A editing on upregulation of genes, while the color represents the gene expression level (the value is averaged if have homologous gene). Interestingly, almost all genes in chemotaxis pathway were up-regulated (Fig. 4c), which revealed that T408A editing event may induce more sensitivity in the bacteria to chemoattractant.

To demonstrate the effect of chemotaxis pathway genes up-regulated, the capillary assay was performed to determine the chemotactic potential of T408A, $T408^{silent}$ and WT strains towards glucose (2.0 mg/mL), serine (10 mg/mL), Fe-Ent (10 μM and 100 μM) and PBS buffer (represent random diffusion). The relative (to glucose) chemotaxis response for each strain was calculated, and the data showed that T408A strain comparing to $T408^{silent}$ strain had increased the sensitivity of Fe-Ent (both 10 μM and 100 μM level), whereas the chemotactic ability of serine did not show significant difference (Fig. 4d).

Based on the results of chemotaxis response, two of MCPs (methyl-accepting chemotaxis proteins, XOC_2282 and XOC_2291) were expressed and purified to determine whether the MCPs directly interact with $FeCl_3$ or Fe-Ent using Fortebio Octet RED system (Fig. 5). In association and dissociation phases, the association curves of Fe-Ent (green and blue) exceeded the 0 nm line, which shows that MCPs could bind Fe-Ent directly (Fig 5c and 5d). Whereas, the curves of $FeCl_3$ (bronzing) were lower than 0 nm line (Fig 5a and 5b), which conferred the lack of potential binding affinity between the MCPs and Fe^{3+}. In addition, the binding kinetic analysis demonstrated that the MCPs indeed directly bind Fe-Ent rather than Fe^{3+}, with a K_D

value of 1-10μM level (Table 1). In summary, T408A editing event could enhance the sensitivity of bacterial chemotaxis towards Fe-Ent, thus it directly binds with MCPs to stimulate the bacterial sense of iron.

T408A editing contributes to virulence of *Xoc*

Since the importance of iron uptake and chemotaxis for virulence (20-23), leaves of six-week-old susceptible rice cv. Yuanfengzao were inoculated with *Xoc* strains and mutants (Fig. 6a). At 14 days after inoculation, lesions induced by the T408A mutant were 3.17 cm; this was significantly longer than 1.88 cm lesions induced by $T408^{silent}$ and 2.33 cm of WT strain (Fig. 6b). Compare to WT, there was a clear decrease in the virulence of the $T408^{silent}$ mutant, suggesting the level of T408A RNA editing contributes to virulence. Furthermore, *in planta* growth assays indicated that the colonial population of the T408A mutant was significantly higher than the other strains, besides the colonizing capacity of $T408^{silent}$ was obviously lower than WT strains (Fig. 6c). Overall, the T408A editing event could improve the niche adaption of iron depletion; moreover, the increase of iron uptake efficiency mediated by T408A editing could significantly enhance the virulence of the *Xoc* strain.

DISCUSSION

The detection of iron concentration is necessary in bacteria including pathogenic bacteria to determine their successful survival and infection in the environment (2). Currently, the most well studied example is Fur, which is an important cytoplasmic regulator of iron homeostasis in bacteria (24). It can regulate expression of beneficial or detrimental genes based on the limitation of ferrous iron (24). Interestingly, our

recent study (11) and this study suggest that bacteria may use our newly identified strategy (post-transcriptional A-to-I modification) to regulate the uptake of the ferrous iron efficiently without the regulation by Fur.

A-to-I RNA editing, which is catalyzed by the adenosine deaminase, acts on RNA (ADAR) family of enzymes, is one of the most prevalent type of post-transcriptional modification in metazoans (25, 26). In eukaryotes, this modification has been proved to play an important role in all aspects of regulatory processes such as splicing, microRNA targeting and processing and mRNA stability (27). The editing of nuclear protein-coding transcripts was long thought to be absent in bacterial species until recently that several cases were discovered (11, 12). From our recent and this study, we found that bacteria may use A-to-I editing as an alternative strategy in iron metabolic uptake, as the editing event level can precisely regulate the RNA and the protein sequence within relatively short physiological time scales (12) comparing with the traditional switch “on” and “off” regulation by Fur regulators.

Iron is an essential for bacteria, however, iron excess is also harmful to organisms. To sense the iron is limited or excessed, many bacteria employ the ferric uptake regulator (Fur) to regulate cellular Fe^{2+} levels (28). When at high levels, Fe^{2+} acts as a co-repressor forming a Fur-Fe^{2+} homodimer that binds to *cis*-regulatory element of iron uptake-associated genes to repress their transcription (29). In contrast, at low Fe^{2+} levels, the Fur-Fe^{2+} homodimer is relieved to clear the promoter region and allowing gene expression (28). Previous report has revealed that Fur-mediated regulation controls the expression of dozens of genes including some virulence factors

(30). This result suggests that the change of the regulation of Fur will cause huge impact on all aspect of bacteria.

Because of the double-edge sword effect of iron for bacteria (2), an efficient and precise mechanism to regulate iron absorption is necessary. Our study revealed that in *X. oryzae* pv. *oryzacola*, XfeA is a TBDR that mediates Fe-Ent transport across the outer membrane (Fig. 7). Under low iron concentrations, the percentage of A-to-I editing of the *xfeA* was increased, causing changes in the 3D structure of XfeA, which is facilitating iron to pass through the XfeA channel without any interference to the Fe-Ent ligand (Fig. 7). However, under high iron concentration, the percentage of A-to-I modification to *xfeA* was reduced, thereby restricting the Fe-Ent to pass iron through the channel of XfeA (Fig. 7). The signal of changed concentration of Fe-Ent was received by MCP at cytoplasmic membrane, which modulated the expression of a number of chemotaxis related genes as identified by RNA-seq and direct binding kinetic analysis. Besides the editing is flexible and immediate (31), thus making the modification event like an inching-switch instead of switch on/off regulation. Based on these findings, it was hypothesized that this mechanism evolved due to adaptation of bacteria in the changing environment.

MCPs, which are involved in the regulation of diverse aspects of cellular activities, are the predominant chemoreceptors in bacteria (32). A typical MCP contains a ligand-binding domain (LBD), which can recognize their ligands directly (33). Many types of ligands such as serine, maltose, oxygen and irons have been proven to bind the MCPs, thereafter, transduce the signal to the downstream genes

(34). In this study, we found that rather inorganic Fe^{3+}, Fe-Ent can bind to MCP directly. To the best our knowledge, this is the first report that MCP can bind to Fe-Ent directly. Moreover, we also found that the signal of MCP binding to Fe-Ent can be transduced to regulate the activity of CheA and other chemotaxis related genes, confirmed by RNA-seq and qPCR (Fig. 4, Table S3). Based on the model of *E.coli*, the MCPs-CheW-CheA may form a signaling kinase complex and transduce the signal to response regulator CheY by phosphorylation. Phosphatase CheZ, methyltransferase CheR and methylesterase CheB constitute the regulator and MCPs modification pathway, therefore the seven different types of proteins constituting the chemotaxis signal transduction system in prokaryotes (35). From the above, this regulation and its consequences on the chemotaxis system can be served as precise sensory adaptation in bacterial chemotaxis through A-to-I RNA editing. The evidence of directly binding between MCP and Fe-Ent (instead of Fe^{3+}) can help to research of the iron chemotaxis and the key interacting residues could be found with further studies.

Overall, the results of this study revealed the significance of the A-to-I RNA editing for bacterial iron metabolic uptake. Using the RNA-seq and Sanger sequence, we demonstrated the rate of A-to-I modification rise with the depletion of environmental iron concentration, and the T408A editing event can improve the bacterial iron uptake capacity and the tolerance to iron depletion. We provide the evidence that MCPs could bind to Fe-Ent directly, and that T408A editing event plays an important role in the chemotaxis. Virulence and colonization assay of susceptible rice provide further evidences about the T408A editing event could improve the niche

adaption of iron depletion. Interestingly, we found that T408A editing in our study is *tad*A independent. Recently, Gao and his colleagues found that there are other types of A-to-I editing enzymes existing in bacterial genomes (14). Strikingly, we can't find any homologs of these genes in the genome of *Xoc*. This result suggests that there should be another unknown A-to-I editing gene existing in the genome of *Xoc*.

In conclusion, we have identified a new inching-switch-like mechanism by which pathogens may absorb iron better in order to compete with the hosts, furthermore the level of RNA editing is regulated by environmental iron concentration.

MATERIALS AND METHODS

Bacterial strains, plasmids, and plant materials

The bacterial strains and plasmids used in this study are described in Table S1. *Xoc* BLS256 is the wild-type (WT) strain of *X. oryzae* pv. *oryzicola*. T408^{silent} contains a synonymous mutation (TACG to TACA) in *xfeA* that blocks post-transcriptional A-to-I modification at amino acid 408. Strain T408A is a derivative of BLS256 containing a mutation (TACG to TGCG) that changed the threonine residue at amino acid 408 to alanine. Strain BL21-2282 and BL21-2291 is a derivative of BL21 that harbor the pET-30a::*xoc_2282* and pET-30a::*xoc_2291* to express protein of MCPs (XOC_2282 and XOC_2291). Further details of strains and plasmids are provided in Table S1.

Escherichia coli strains were cultured in Luria-Bertani (LB) medium at 37°C (36). *Xoc* BLS256 strains were cultured in nutrient broth (NB, 1% peptone, 0.5% yeast extract, 1% sucrose) or in NB containing 1.5% agar at 28°C. The final concentrations

of the antibiotics were as follows: kanamycin, 25 μg/mL; cephalexin, 40 μg/mL and streptonigrin (SNG) 1 μg/mL. Filter sterilized 2, 2'-dipyridyl (DP) and $FeCl_3$ as iron chelator and supplements were prepared as 10mM stocks, added in 100- or 200-fold volume NB medium when used.

Rice seeds were obtained from the International Rice Research Institute. All rice plants were grown at 28°C with a 12-h photoperiod in a greenhouse located at Shanghai Jiao Tong University.

Bacterial mutant and strain construction

Construction of bacterial mutant strains was performed as described by Baba (37) with the following modifications. For site-directed mutagenesis, plasmids were modified with the Fast Mutagenesis System (Transgen Biotech, Beijing, China) to obtain clones containing the point mutations (T408A and $T408^{silent}$). Fragments encoding *xfeA* in *Xoc* BLS256 were amplified with the corresponding *xoc3486* F/R primers (Table S2), digested with *Sal*I/*Xho*I, and subcloned into the *Sal*I/*Xho*I site of pKMS1(38). Mutations were introduced by PCR amplification with overlapping primers containing the target A-G point mutations as follows: T408A F/R and $T408^{silent}$ F/R (Table S2). The PCR product was digested with the DMT enzyme supplied in the Fast Mutagenesis System, and plasmids containing A-G or G-A point mutations were transformed into DMT competent cells and verified by Sanger sequencing. Sequence substitutions were performed by double homologous recombination similar to the gene knockouts. In brief, for the T408A and $T408^{silent}$ strains, the point mutation carried fragments in pKMS1 were separately introduced

into *Xoc* BLS256 by electroporation (Bio-Rad Laboratories Inc., Hercules, CA, USA) and subjected to kanamycin selection. A single transformant colony with kanamycin resistance was picked and cultured for 8 h in NB medium without kanamycin and sucrose; 10-fold dilutions were then inoculated to nutrient agar (NA) with 15% sucrose to obtain sucrose-insensitive clones.

To construct the protein-expressing strain (BL21-xoc2282 and BL21-xoc2291), the whole-length fragments of *xoc_2282* and *xoc_2291* were amplified with the *Pfu* polymerase (TransGen Biotech, Beijing, China) using the xoc2282 and xoc2291 F/R primers (Table S2). These fragments were cloned, digested with *BamHI/Hind*III, and the two fragments were ligated into the *BamHI/Hind*III site of expression vector pET-30a (+). The protein expression fragments in pET-30a (+) were separately introduced into BL21 (DE3) by chemical transformation. In brief, 50μl BL21 (DE3) chemically competent cell added 2.5μl of DNA, and then keep in the ice bath for 30 min. After heat-shock at 42℃ for 45 sec, the tube was placed in the ice bath for 2 min, and then add a 500μl LB medium for reviving and shaking for 1 h. 200μl of transforming cell were inoculated to LB agar and cultured overnight to obtain protein expressing clones.

RNA secondary structure prediction

A sequence consisting of residues from -25 to +25 bp from the edited site was extracted for prediction of RNA secondary structure with the RNAfold web server (http://rna.tbi.univie.ac.at/cgi-bin/RNAWebSuite/RNAfold.cgi) based on minimum free energy.

3D structure prediction

For 3D modeling, the sequence of the XfeA was input into the RCSB Protein Data Bank (PDB) to search for templates that could be used for homology modeling. The X-ray structure of *A. baumannii PiuA (PDB ID: 5FP1)* was used as the template for homology modeling of XfeA by an in-house program SAMM (39) with energy minimization using AMBER10 force field (40). Default values were used for the iteration limit and RMS gradient test.

Bacterial growth assays in response to iron deplete stress

Optical density (OD) was measured with a Bioscreen C instrument (Labsystem, Helsinki, Finland). For each well, 99 μL of NB medium with or without DP was inoculated with 1 μL of an overnight culture (1×10^9 CFU/mL). The OD values at 420-580 nm were measured every 15 min for 24 h with continuous shaking at 28℃. Four independent replicates were carried out in this study. Pairwise comparisons of growth curve (Logistic curve fitted by OD values) for each strain and growth condition were analyzed with the *F*-test against the curve obtained for $T408^{silent}$. Data progressing, fitting and drawing with OriginPro 2018C version 9.5.1.195.

Cellular iron concentration

Xoc cellular iron concentrations were detected by inductively coupled plasma-optical emission spectroscopy (ICP-OES, Optima 8000, PerkinElmer, MA USA), as reported previously (2, 41). The bacterial cells were grown to an OD_{600} of 1.0 in NB medium. Bacterial cells were collected by centrifugation and washed with

sterilized PBS buffer three times, and the stains were then inoculated into 2-fold volume of fresh NB medium added 50 μM DP or 100 μM $FeCl_3$. After 3-5 h of growth (until OD_{600}=0.6), cells were harvested by centrifugation and washed three times with sterilized PBS buffer. The pelleted cells were oven-dried at 65□ for 48 h, and digested with the acid solution (HNO_3–$HClO_4$, 4:1, v/v). The digest was then transferred to a 25 mL volumetric tube and diluted to 25 mL with deionized water. The iron atom content was then measured by ICP-OES. Samples did not treat with the acid solution were used as parallel controls. The iron concentration of strain was calculated by dividing the iron atom value for every 10^9 *Xoc* cells.

Streptonigrin survival assays

Streptonigrin survival assays were performed as described previously with minor modifications (42). Log-phase (OD_{600}=0.6) *Xoc* cells were harvested by centrifugation, washed with 0.01M PBS buffer (NaCl 8.5g/L, Na_2HPO_4 2.2g/L, NaH_2PO_4 0.4g/L, pH=7.0) three times, and exposed to 1μg/mL streptonigrin for 16h at 28°C. Cultures were subjected to serial 10-fold dilutions, inoculated to NA, and colonies were counted after a 48 h-incubation at 28 °C. The percentage of survival rate was calculated by comparing the treated group without streptonigrin. This assay was performed in triplicate.

Exposure of *Xoc* strains to iron chelator/supplement and RNA extraction

Xoc strains were incubated as described previously with minor modifications (43). BLS256 WT strain were incubated at 28□ to OD_{600}=1.0 in NB medium with DP or $FeCl_3$. Aliquots were withdrawn and pelleted by centrifugation at 4°C. Each cell pellet

was washed two times in cold PBS buffer, and total RNA was then extracted with the RNeasy Protect Bacteria Mini Kit (Qiagen). Two biological replicates were examined for this experiment.

qRT-PCR and PCR for cDNA

RNA was purified with EasyPure RNA Kit (Transgen Biotech) as recommended by the manufacturer. RNA (1 μg) was used to synthesis cDNA with Magic 1st cDNA Synthesis Kit (With dsDNase) (Magic Biotech, Hangzhou, China). Then, 20 μl of synthesized cDNA was diluted to 100 μl and used for qRT□PCR with Magic SYBR Green qPCR Mix (Magic Biotech) and the ABI 7500 quantitative PCR system (Applied Biosystems, Foster City, CA). Normalized expression levels of target genes were calculated relative to rpoD using the ΔΔCT method, where CT is the threshold cycle. Three independent biological replicates were carried out in this study.

PCR (c T408 F/R primers, Table S2) was performed to sequence the *xfeA* transcript from cDNA samples of *Xoc* BLS256. The chromatograms were visualized by Chromas Lite (Technelysium, Brisbane, Australia), and the frequency of editing was estimated by ratiometric A/G measurement.

mRNA purification and cDNA synthesis for RNA sequence

Total RNA (10 μg/sample) was isolated and treated with the MICROBExpress Bacterial mRNA Enrichment kit (Ambion) and RiboMinus™ Transcriptome Isolation Kit (Bacteria) (Invitrogen) as recommended by the manufacturers. Bacterial mRNAs were suspended in RNase-free water (15 μL) and chemically fragmented to 200-250 bp using 1X fragmentation solution (Ambion) for 2.5 min at 94°C. cDNA was

generated according to instructions provided in the SuperScript Double-Stranded cDNA Synthesis Kit (Invitrogen). Briefly, mRNA samples were mixed with 100 pmol of random hexamers, incubated at 65°C for 5 min, chilled in ice, and mixed with 4 μL of First-Strand Reaction Buffer (Invitrogen), 2 μL 0.1 M DTT, 1 μL 10 mM RNase-free NTP mix, and 1 μL SuperScript III reverse transcriptase (Invitrogen); mixtures were then incubated at 50°C for 1 h. To generate the second strand, the following Invitrogen reagents were added and samples were incubated at 16 °C for 2.5 h: 51.5 μL RNase-free water, 20 μL second-strand reaction buffer, 2.5 μL 10 mM RNase-free dNTP mix, 50 U DNA polymerase, and 5 U RNase H.

RNA sequencing and RNA-seq data analysis

The Illumina Paired End Sample Prep kit was used to create RNA-Seq libraries as described previously (44). After removing low quality reads and adaptors, RNA-Seq reads were aligned to the corresponding *Xoc* BLS256 genome using Tophat 2.0.7 (45), allowing for a maximum of two mismatched nucleotides. If reads mapped to more than one location, only the site showing the highest score was retained. Reads mapping to rRNA and tRNA regions were removed from further analysis. After obtaining read numbers from every sample, edgeR with TMM normalization method was used to determine differentially expressed genes (DEGs). Significant DEGs (FDR value < 0.01) were selected for further analysis, and Cluster 3.0 and Treeview 1.1.6 were used to generate heatmap clusters based on the RPKM values (46, 47).

Capillary chemotaxis assay

For the chemotaxis assay, the capillary method was performed as described

previously with several modifications (20). Briefly, *Xoc* strains were grown in NB medium to OD_{600} = 1.0. The cells were centrifuged at 800×g for 6 min, washed with PBS buffer three times and resuspended. Sterilized capillary tubes containing 0.22-μm filter-sterilized attractant 2.0 mg/mL glucose, 10 mg/mL serine, 10μM Fe-Ent, 100μM Fe-Ent and 0.01M PBS buffer (as negative control) were incubated with cell suspension of *Xoc* strains at 28 ºC for 4 h. To determine the CFU of strains in the capillaries, the content of the capillary was serially 10-fold dilution plated on PBS buffer (The diagram see Fig. S3). Relative chemotaxis response (relative to glucose for each strain respectively) was calculated by the number of migrated bacterial cells in the capillary, exclude the cell number of PBS buffer containing because of bacterial random motility or diffusion.

Direct binding kinetic analysis of MCPs to $FeCl_3$ and Fe-Ent

For the protein (XOC_2282 and XOC_2291) expression and purification, 6×His-tag recombinant protein was expressed by constructing the expression vector (pET-30a) and purified from BL21 strain (Table S1) following the protocol of the BeyoGoldTM His-tag purification Resin (Beyotime, Shanghai, China), and then the proteins were concentrated with molecular sieve (Millipore China, Shanghai, China). The binding kinetic analysis was performed as described previously with several modifications (48). In brief, $FeCl_3$ or Fe-Ent was dissolved with PBS buffer at the concentration of 50μM. Similarly, the products of protein concentration were diluted with PBS buffer at the concentration of 10μM. After baseline step, the His-tag labeled protein (XOC_2282 and XOC_2291) were bound to the Octet Red biosensors

(Ni-NTA sensor), then washed and blocked by PSA buffer (0.2% PSA and 0.02% Tween-20 dissolve in PBS buffer), the biosensors were incubated for 300 sec with 50μM $FeCl_3$ or Fe-Ent buffer to association, whereas the biosensors were incubated with the PBS buffer for 600 sec to determine the dissociation rate. The Octet Data Analysis HT software version 12 was used to fit the curve and calculate the value of the dissociation constant (K_D).

Plant inoculation assays

Bacterial suspensions (OD_{600}=0.6) were used to inoculate 6-week-old rice with needleless syringes, and lesion lengths were measured 14 days after inoculation. Thirteen leaves were inoculated and evaluated for each *Xoc* strain.

For colony counting, three leaves, each infected with one *Xoc* strain, were excised around the inoculation site and crushed with sterile beads. Each suspension was subjected to a 10-fold serial dilution, and 5 μL aliquots from 10^{-1} to 10^{-6} dilutions were inoculated to NA with cephalexin. Plates were incubated at 28°C until individual colonies could be counted; statistical analysis was used to calculate viable bacteria per leaf.

Data Availability

All sequence data generated in this study are deposited in NCBI under BioProject number: PRJNA673071.

ACKNOWLEDGEMENTS

We thank Prof. Fu-Zhou Xu for providing Fe-Ent. We thank Prof. Wei Qian for his valuable suggestion. This work was supported by National Key R&D Program of

China (2018YFD0201202, 2017YFD0201108), the Agri-X Interdisciplinary Fund of Shanghai Jiao Tong University (Agri-X2017010), the State Key Laboratory for Biology of Plant Diseases and Insect Pests (SKLOF201802), Shanghai Committee of Science and Technology (19390743300), National Natural Science Foundation of China (31200003, 31770772) and Joint Research Funds for Translational Medicine at Shanghai Jiao Tong University (ZH2018ZDA06).

REFERENCES

1. Skaar EP. 2010. The battle for iron between bacterial pathogens and their vertebrate hosts. PLoS Pathog 6**:**e1000949.
2. Wang L, Pan Y, Yuan Z-H, Zhang H, Peng B-Y, Wang F-F, Qian W. 2016. Two-component signaling system VgrRS directly senses extracytoplasmic and intracellular iron to control bacterial adaptation under iron depleted stress. PLoS Pathog 12**:**e1006133.
3. Hood MI, Skaar EP. 2012. Nutritional immunity: transition metals at the pathogen–host interface. Nat Rev Microbiol 10**:**525-537.
4. Kehl-Fie TE, Skaar EP. 2010. Nutritional immunity beyond iron: a role for manganese and zinc. Curr Opin Chem Biol 14**:**218-224.
5. Fischbach MA, Lin H, Liu DR, Walsh CT. 2006. How pathogenic bacteria evade mammalian sabotage in the battle for iron. Nat Chem Biol 2**:**132-138.
6. Raines DJ, Moroz OV, Blagova EV, Turkenburg JP, Wilson KS, Duhme-Klair A-K. 2016. Bacteria in an intense competition for iron: Key component of the Campylobacter jejuni iron uptake system scavenges enterobactin hydrolysis product. Proc Natl Acad Sci U S A 113**:**5850-5855.
7. Hider RC, Kong X. 2010. Chemistry and biology of siderophores. Nat Prod Rep 27**:**637-657.
8. Ryan RP, Vorhölter F-J, Potnis N, Jones JB, Van Sluys M-A, Bogdanove AJ, Dow JM. 2011. Pathogenomics of *Xanthomonas*: understanding bacterium–plant interactions. Nat Rev Microbiol 9**:**344-355.
9. **Schalk IJ, Mislin GL, Brillet K.** 2012. Structure, function and binding selectivity and stereoselectivity of siderophore–iron outer membrane transporters, p. 37-66, Current topics in membranes, vol. 69. Elsevier.
10. Raymond KN, Dertz EA, Kim SS. 2003. Enterobactin: an archetype for microbial iron transport. Proc Natl Acad Sci U S A 100**:**3584-3588.
11. Nie W, Wang S, He R, Xu Q, Wang P, Wu Y, Tian F, Yuan J, Zhu B, Chen G. 2020. A-to-I RNA editing in bacteria increases pathogenicity and tolerance to oxidative stress. PLoS Pathog 16**:**e1008740.
12. Bar-Yaacov D, Mordret E, Towers R, Biniashvili T, Soyris C, Schwartz S, Dahan O,

Pilpel Y. 2017. RNA editing in bacteria recodes multiple proteins and regulates an evolutionarily conserved toxin-antitoxin system. Genome Res 27:1696-1703.

13. Garrett S, Rosenthal JJ. 2012. RNA editing underlies temperature adaptation in K^+ channels from polar octopuses. Science 335:848-851.

14. Gao L, Altae-Tran H, Böhning F, Makarova KS, Segel M, Schmid-Burgk JL, Koob J, Wolf YI, Koonin EV, Zhang F. 2020. Diverse enzymatic activities mediate antiviral immunity in prokaryotes. Science 369:1077-1084.

15. Buchanan SK, Smith BS, Venkatramani L, Xia D, Esser L, Palnitkar M, Chakraborty R, Van Der Helm D, Deisenhofer J. 1999. Crystal structure of the outer membrane active transporter FepA from *Escherichia coli*. Nat Struct Biol 6:56-63.

16. Ma L, Kaserer W, Annamalai R, Scott DC, Jin B, Jiang X, Xiao Q, Maymani H, Massis LM, Ferreira LC. 2007. Evidence of ball-and-chain transport of ferric enterobactin through FepA. J Biol Chem 282:397-406.

17. Newton SM, Igo JD, Scott DC, Klebba PE. 1999. Effect of loop deletions on the binding and transport of ferric enterobactin by FepA. Mol Microbiol 32:1153-1165.

18. Moynié L, Luscher A, Rolo D, Pletzer D, Tortajada A, Weingart H, Braun Y, Page MG, Naismith JH, Köhler T. 2017. Structure and function of the PiuA and PirA siderophore-drug receptors from *Pseudomonas aeruginosa* and *Acinetobacter baumannii*. Antimicrob Agents Chemother 61.

19. Yeowell HN, White JR. 1982. Iron requirement in the bactericidal mechanism of *streptonigrin*. Antimicrob Agents Chemother 22:961-968.

20. Kumar Verma R, Samal B, Chatterjee S. 2018. *Xanthomonas oryzae* pv. *oryzae* chemotaxis components and chemoreceptor Mcp2 are involved in the sensing of constituents of xylem sap and contribute to the regulation of virulence□associated functions and entry into rice. Mol Plant Pathol 19:2397-2415.

21. Yao J, Allen C. 2006. Chemotaxis is required for virulence and competitive fitness of the bacterial wilt pathogen *Ralstonia solanacearum*. J Bacteriol 188:3697-3708.

22. Garvis S, Munder A, Ball G, De Bentzmann S, Wiehlmann L, Ewbank JJ, Tümmler B, Filloux A. 2009. Caenorhabditis elegans semi-automated liquid screen reveals a specialized role for the chemotaxis gene *cheB2* in *Pseudomonas aeruginosa* virulence. PLoS Pathog 5:e1000540.

23. Brown JS, Gilliland SM, Holden DW. 2001. A *Streptococcus pneumoniae* pathogenicity island encoding an ABC transporter involved in iron uptake and virulence. Mol Microbiol 40:572-585.

24. Hassan HM, Troxell B. 2013. Transcriptional regulation by Ferric Uptake Regulator (Fur) in pathogenic bacteria. Front Cell Infect Microbiol 3:59.

25. Bazak L, Haviv A, Barak M, Jacob-Hirsch J, Deng P, Zhang R, Isaacs FJ, Rechavi G, Li JB, Eisenberg E. 2014. A-to-I RNA editing occurs at over a hundred million genomic sites, located in a majority of human genes. Genome Res 24:365-376.

26. Palladino MJ, Keegan LP, O'Connell MA, Reenan RA. 2000. A-to-I pre-mRNA editing in *Drosophila* is primarily involved in adult nervous system function and integrity. Cell 102:437-449.

27. Schaffer AA, Kopel E, Hendel A, Picardi E, Levanon EY, Eisenberg E. 2020. The cell line A-to-I RNA editing catalogue. Nucleic Acids Res 48:5849-5858.

28. Hantke K. 2001. Iron and metal regulation in bacteria. Curr Opin Microbiol 4:172-177.
29. Chen Z, Lewis KA, Shultzaberger RK, Lyakhov IG, Zheng M, Doan B, Storz G, Schneider TD. 2007. Discovery of Fur binding site clusters in Escherichia coli by information theory models. Nucleic Acids Res 35:6762-6777.
30. McHugh JP, Rodríguez-Quiñones F, Abdul-Tehrani H, Svistunenko DA, Poole RK, Cooper CE, Andrews SC. 2003. Global iron-dependent gene regulation in *Escherichia coli* A new mechanism for iron homeostasis. J Biol Chem 278:29478-29486.
31. Hanswillemenke A, Kuzdere T, Vogel P, Jékely Gsr, Stafforst T. 2015. Site-directed RNA editing *in vivo* can be triggered by the light-driven assembly of an artificial riboprotein. J Am Chem Soc 137:15875-15881.
32. Ud-Din AIMS, Roujeinikova A. 2017. Methyl-accepting chemotaxis proteins: a core sensing element in prokaryotes and archaea. Cell Mol Life Sci 74:3293-3303.
33. Milburn MV, Prive GG, Milligan DL, Scott WG, Yeh J, Jancarik J, Koshland DE, Kim S-H. 1991. Three-dimensional structures of the ligand-binding domain of the bacterial aspartate receptor with and without a ligand. Science 254:1342-1347.
34. Muok AR, Deng Y, Gumerov VM, Chong JE, DeRosa JR, Kurniyati K, Coleman RE, Lancaster KM, Li C, Zhulin IB. 2019. A di-iron protein recruited as an Fe [II] and oxygen sensor for bacterial chemotaxis functions by stabilizing an iron-peroxy species. Proc Natl Acad Sci U S A 116:14955-14960.
35. Wuichet K, Zhulin IB. 2010. Origins and diversification of a complex signal transduction system in prokaryotes. Science signaling 3:ra50.
36. **Maniatis T, Fritsch EF, Sambrook J.** 1982. Molecular cloning: a laboratory manual, vol. 545. Cold spring harbor laboratory Cold Spring Harbor, NY.
37. Baba T, Ara T, Hasegawa M, Takai Y, Okumura Y, Baba M, Datsenko KA, Tomita M, Wanner BL, Mori H. 2006. Construction of *Escherichia coli* K□12 in□frame, single□gene knockout mutants: the Keio collection. Mol Syst Biol 2:2006.0008.
38. Xie G-L, Zhang G-Q, Liu H, Lou M-M, Tian W-X, Li B, Zhou X-P, Zhu B, Jin G-L. 2011. Genome sequence of the rice-pathogenic bacterium *Acidovorax avenae* subsp. *avenae* RS-1. J Bacteriol 193:5013-5014.
39. Wang J-F, Wei D-Q, Lin Y, Wang Y-H, Du H-L, Li Y-X, Chou K-C. 2007. Insights from modeling the 3D structure of NAD (P) H-dependent D-xylose reductase of *Pichia stipitis* and its binding interactions with NAD and NADP. Biochem Biophys Res Commun 359:323-329.
40. Vanommeslaeghe K, Hatcher E, Acharya C, Kundu S, Zhong S, Shim J, Darian E, Guvench O, Lopes P, Vorobyov I. 2010. CHARMM general force field: A force field for drug□like molecules compatible with the CHARMM all□atom additive biological force fields. J Comput Chem 31:671-690.
41. Desrosiers DC, Sun YC, Zaidi AA, Eggers CH, Cox DL, Radolf JD. 2007. The general transition metal (Tro) and Zn^{2+} (Znu) transporters in Treponema pallidum: analysis of metal specificities and expression profiles. Mol Microbiol 65:137-152.
42. Si M, Zhao C, Burkinshaw B, Zhang B, Wei D, Wang Y, Dong TG, Shen X. 2017. Manganese scavenging and oxidative stress response mediated by type VI secretion system in *Burkholderia thailandensis*. Proc Natl Acad Sci U S A 114:E2233-E2242.
43. Upadhya R, Campbell LT, Donlin MJ, Aurora R, Lodge JK. 2013. Global transcriptome

profile of *Cryptococcus neoformans* during exposure to hydrogen peroxide induced oxidative stress. PLoS ONE 8**:**e55110.

44. Fang Y, Wang H, Liu X, Xin D, Rao Y, Zhu B. 2019. Transcriptome analysis of *Xanthomonas oryzae* pv. *oryzicola* exposed to H2O2 reveals horizontal gene transfer contributes to its oxidative stress response. PLoS ONE 14**:**e0218844.

45. Trapnell C, Pachter L, Salzberg SL. 2009. TopHat: discovering splice junctions with RNA-Seq. Bioinformatics 25**:**1105-1111.

46. Saldanha AJ. 2004. Java Treeview—extensible visualization of microarray data. Bioinformatics 20**:**3246-3248.

47. de Hoon MJL, Imoto S, Nolan J, Miyano S. 2004. Open source clustering software. Bioinformatics 20**:**1453-1454.

48. Li H, Tao Y, Zhao P, Ban X, Zhi D, Li G, Wang F, Yang X, Huai L. 2015. Recognization of receptors on bone marrow-derived dendritic cells bound with *Pholiota nameko* polysaccharides. Int J Biol Macromol 72**:**649-657.

Figure Legends

Figure 1. Analysis of the *xfeA* (T408A) A-to-I RNA editing level by Sanger sequencing. (a) Sequence analysis of cDNA in edited regions of wild-type (WT) in NB medium, NB+50μM 2,2'-dipyridyl (DP, as an iron chelator), NB+100μM DP, NB+150μM DP, NB+100μM $FeCl_3$, and *ΔtadA* (tRNA-specific adenosine deaminase) strain in NB medium. PCR fragments were obtained from cDNA (mRNA) using primers described in Methods. Samples were incubated over-night at log-phase and then subjected to Sanger sequencing. Three independent biological replicates were carried out in this study (N.S. represent no significance). (b) The conserved editing TACG motif is framed by the blue frame in the DNA sequence. Chromatograms show editing level in different culture conditions, and the A/G percentage of the edited sequence as determined by Sanger sequencing is indicated (A-to-I editing event site in the red frame). For $T408^{silent}$ strain, the red arrow indicates the DNA mutation site of

TACG to TACA, and to demonstrate the change of motif could block the A-to-I editing on the editing site (red frame).

Figure 2. Homology modeling of XfeA. (a) Homology model of XfeA using PiuA from *A. baumannii* (PDB ID: 5FP1) as the template. The backbone is colored green and magenta at the 22-stranded transmembrane β-barrel and plug domains of the model, respectively. The threonine residue (Thr408) is depicted using spheres. (b) Comparison of hydrogen bonding around the mutation site. The loss of several critical H bonds (in red circle) in the Thr408Ala mutant (right) may disrupt the H-bonding network surrounding Thr408 (left), which may diminish this local tether of this segment. The carbons of the β-barrel are colored green and the plug domains residues are colored magenta in both models.

Figure 3. T408A RNA editing modulates bacterial responses to iron-replete and depleted conditions. (a) Bacterial growth curve of *Xoc* T408A, $T408^{silent}$ and WT in NB medium. Strains were grown in quadruplicate to mid-exponential phase, diluted to OD_{600}=0.1, transferred to fresh NB and placed in a Bioscreen C apparatus at 28°C; (b) Growth in NB supplemented with 50μM 2,2'-dipyridyl. (c) Growth in NB supplemented with 100μM 2,2'-dipyridyl. (d) Growth in NB supplemented with 150μM 2,2'-dipyridyl. Error intervals (light shaded regions) indicate mean ± SE of *n* = 4 replicates. In (a, b, c and d), the F-test against the fitting logistic function obtained for T408A and WT compared with $T408^{silent}$ growth curve, * and ** indicate the

significant difference is lower than 0.05 and 0.01 respectively. (e) Iron content in *Xoc* T408A, T408^{silent} and WT. Bacterial cells were cultured in NB medium added 50μM 2,2'-dipyridyl or 100μM $FeCl_3$. The concentrations of total iron in *Xoc* were measured with inductively coupled plasma spectroscopy (ICP-OES). (f) Survival rates of *Xoc* subjected to 1μg/ml streptonigrin (SNG) treatment. Middle log-phase bacterial cultures (OD_{600} = 0.5) in NB medium (with or without 50μM 2,2'-dipyridyl) were treated with 1μg/ml streptonigrin (SNG) for 24 h and the survival rates were calculated by counting the 10-fold serial dilution colony-forming unit (cfu). In (e and f), error bars represent standard deviations (n = 3), * and ** indicate the significant difference between the samples and the control group T408^{silent} is lower than 0.05 and 0.01 respectively (Student's *t*-test).

Figure 4. The upregulation of a chemotaxis gene pathway, which was detected by RNA-seq, contributes to enhance the sensitivity of Fe-Ent. (a) Volcano plot showing the FDR P-value and fold change of T408A versus T408^{silent}. Red dots indicate the upregulated genes with FDR P < 0.01, while blue dots indicate downregulated genes with FDR P < 0.01. (b) Normalized expression levels of selected chemotaxis pathway genes were calculated relative to rpoD using the ΔΔCT method between T408A and T408^{silent}, where CT is the threshold cycle (all samples normalized to T408^{silent} strain grown on NB). Three independent biological replicates were carried out in this study. The significant difference between T408A and T408^{silent} is lower than 0.01 (**) and 0.001 (***, Student's t-test). (c) The gene expression fold change (indicated by color)

of bacterial chemotaxis pathway and flagellar assembly based on the RNA-seq data. (d) The relative chemotaxis response of *Xoc* strains with different chemoattractants. The relative chemotaxis response value was calculated by the number of migrated bacterial cells. The significant difference was calculated by Student's t-test.

Figure 5. Binding kinetic analysis of MCPs (*xoc_2282* and *xoc_2291*) to $FeCl_3$ (Fig 5a and 5b) or Fe-Ent (Fig 5c and 5d) by Fortebio Octet Red System (ForteBio Analytics Shanghai Co., Ltd.). Real-time association and dissociation analysis of MCPs to $FeCl_3$ or Fe-Ent. MCPs were bound to the Octet Red biosensors (Ni-NTA sensor), and then washed and blocked by PSA buffer, the biosensors were incubated with 50μM $FeCl_3$ or Fe-Ent buffer to association (bronzing: $FeCl_3$; blue: Fe-Ent (XOC_2282); green: Fe-Ent (XOC_2291); and red: fitted curve), and then the biosensors were incubated with the PBS buffer to determine the dissociation rate.

Figure 6. Virulence and *in planta* growth in rice cv.Yuanfengzao. Virulence was assessed by inoculating six-week-old susceptible Yuanfengzao rice plants with *Xoc* strains. (a) Symptoms on rice leaves inoculated with the T408A, $T408^{silent}$ and WT. (b) Leaves (n=13) were inoculated with needleless syringes and evaluated for lesion length 14 days after inoculation. Values represent the mean lesion length ± SD. The cross (×) indicates the abnormal value. The asterisks (*) indicate significant differences between the data obtained for T408A and WT as compared to the $T408^{silent}$ strain (*, $P < 0.05$; ***, $P < 0.001$; ANOVA with Dunnett's

multiple test post-hoc correction compared with T408^{silent}). (c) Population dynamics of T408A T408^{silent} and WT cells *in planta* (means ± SD). Leaves (*n*=3) each infected with one strain of *Xoc*, were excised around the inoculation site and then crushed with sterile beads. Each suspension was subjected to a 10-fold serial dilution, and 10 μl drops from the 10^{-1}–10^{-6} dilutions were placed on NB agar with cephalexin. *, $P < 0.05$; **, $P < 0.01$.

Figure 7. Proposed new inching switch mechanism that bacteria use to dynamically regulate the iron homeostasis by A-to-I modification in *xfeA* adapt to shifty iron concentration. Under iron-depleted or host plant environments, T408A editing level within *xfeA* is enhanced, thus increasing the Fe-Ent uptake, and then rouse the chemotaxis pathway genes to improve the sensitivity, thereby contributing to the fitness of iron deficiency and virulence of the host plant. When *Xoc* under the iron-depleted condition, the A-to-I modification level is reduced.

Appendixes

Figure S1. Normalized expression levels of selected chemotaxis pathway genes and *xfeA* were calculated relative to rpoD using the ΔΔCT method in BLS256 wild-type strain, where CT is the threshold cycle. Three independent biological replicates were carried out in this study.

Figure S2. RNA secondary structure prediction of the T408A mutation in *Xoc* XfeA.

RNA secondary structure analysis (http://rna.tbi.univie.ac.at/) showed that the edited site is embedded within a loop (see arrow).

Figure S3. The diagram of capillary chemotaxis test device and process.

Figure S4. Verifications of the *xfeA* T408A A-to-I RNA editing site by Sanger sequencing (gDNA as the template). Chromatograms show that no A/G mixture exists at the DNA level, and could exclude the possibility of DNA mutation in a subpopulation that is further selected at experimental conditions.

Figure S5. Comparing of A-to-I RNA editing level between the RNA-seq data of T408A and $T408^{silent}$ strain in NB medium with two biological replicates. Because of the DNA site-mutation, the editing level of *xfeA* is 100% and 0% in T408A and $T408^{silent}$ strain respectively (red frame), and verifying the construction of $T408^{silent}$ strain could block the A-to-I RNA editing of *xfeA*.

Table 1. Direct binding kinetics for MCPs binding $FeCl_3$ or Fe-Ent immobilized on Ni-NTA biosensors

Figure	**Protein**	**Compound**	**Conc. (μM)**	**K_D (M)**	**K_{on} ($M^{-1}\cdot s^{-1}$)**	**K_{dis} (s^{-1})**	**R^2**
a	Xoc_2282	$FeCl_3$	50	N.A.	N.A.	N.A.	0
b	Xoc_2291	$FeCl_3$	50	N.A.	N.A.	N.A.	0
c	Xoc_2282	Fe-Ent	50	$(4.88\pm1.02)\times10^{-6}$	$(5.21\pm0.08)\times10^{2}$	$(2.54\pm0.03)\times10^{-3}$	0.9962
d	Xoc_2291	Fe-Ent	50	$(8.74\pm2.35)\times10^{-6}$	$(2.78\pm0.04)\times10^{2}$	$(2.43\pm0.02)\times10^{-3}$	0.9335

Note: N.A. means the parameter is not available for the interaction combination.

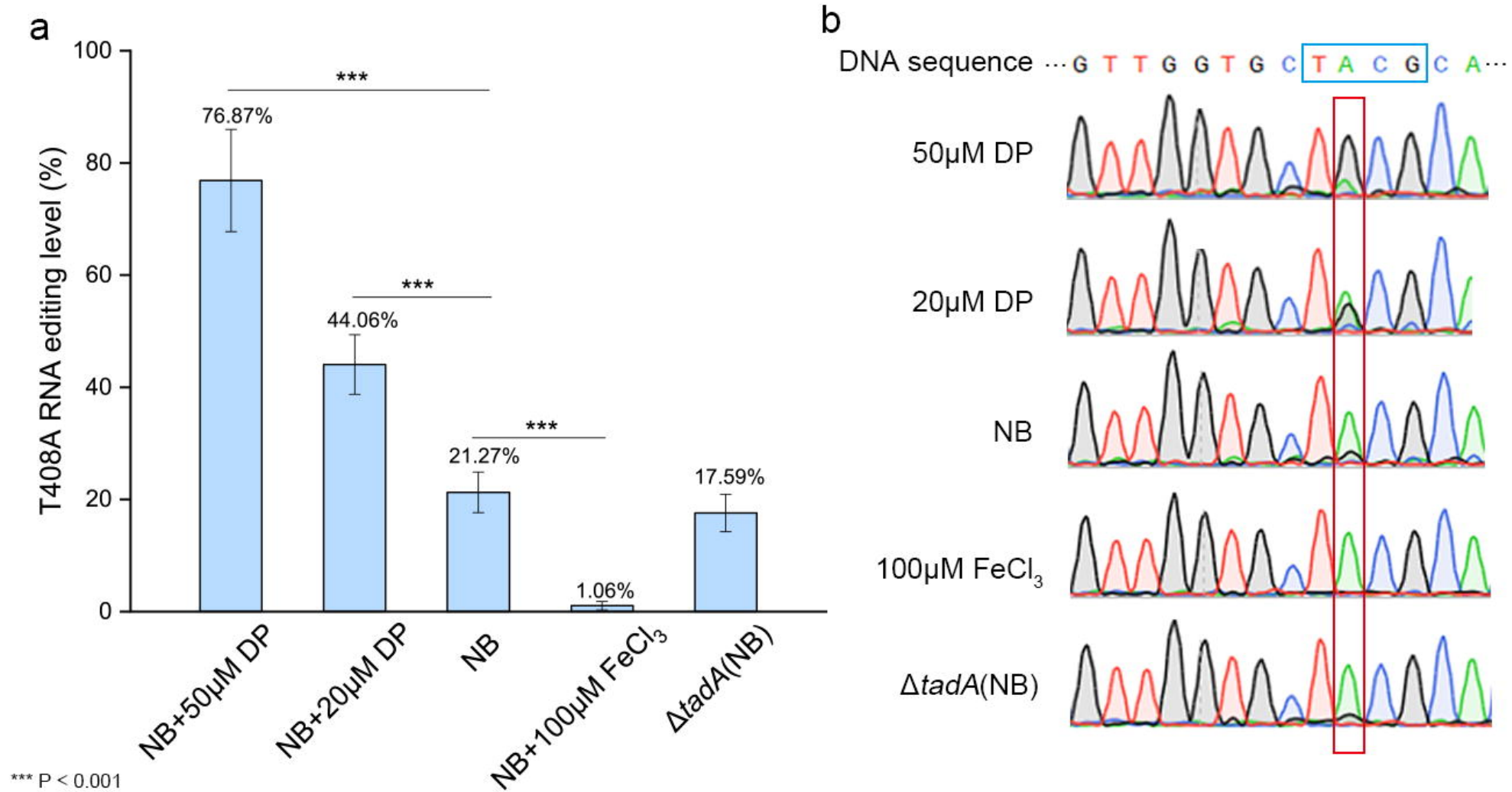
a
T408A RNA editing level (%)
100
80
60
40
20
0
***
76.87%
44.06%
21.27%
1.06%
17.59%
NB+50μM DP
NB+20μM DP
NB
NB+100μM FeCl3
ΔtadA(NB)
*** P < 0.001
b
DNA sequence ···G T T G G T G C T A C G C A···
50μM DP
20μM DP
NB
100μM FeCl3
ΔtadA(NB)

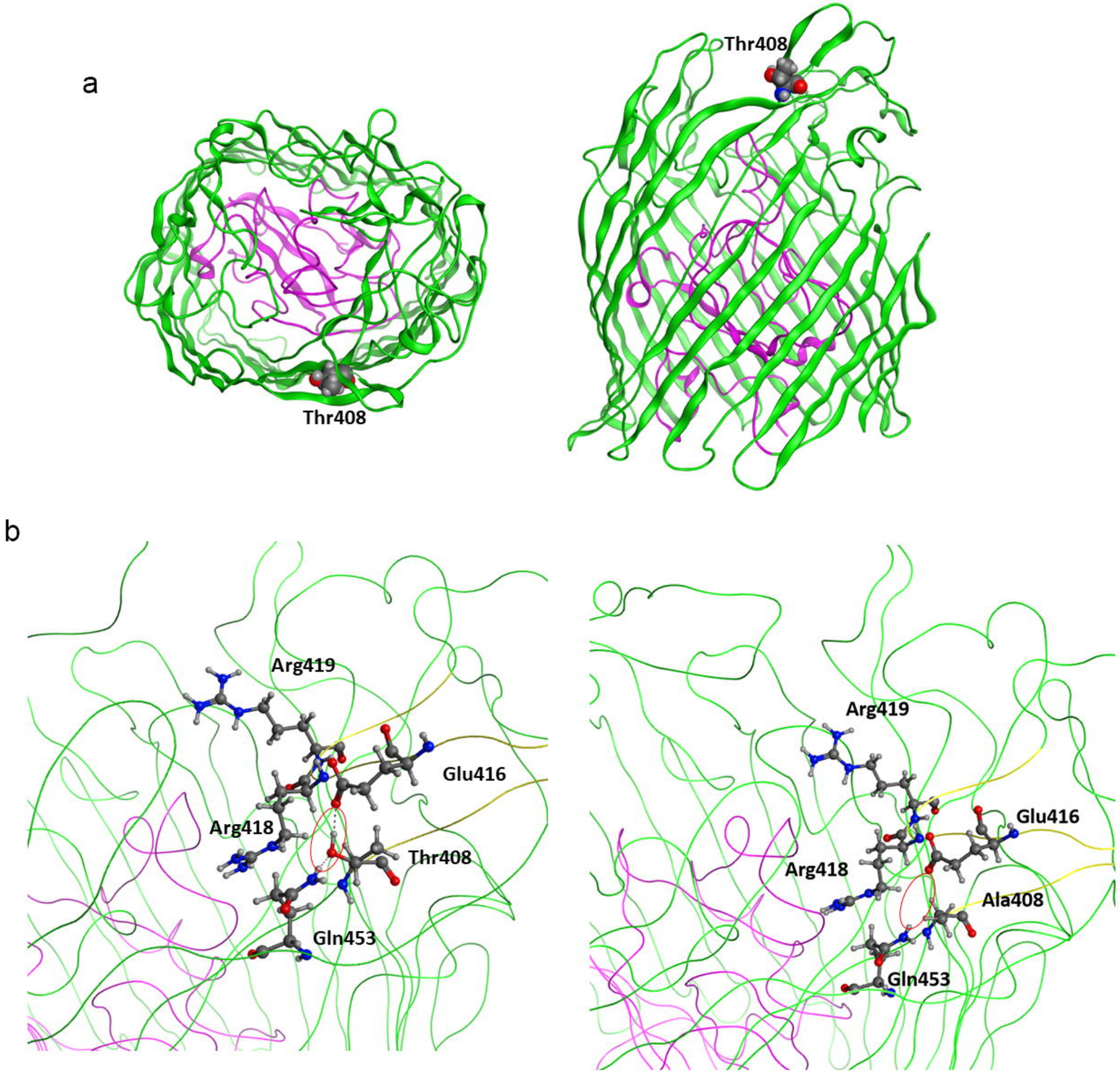
a
Thr408
Thr408
b
Arg419
Glu416
Arg418
Thr408
Gln453
Arg419
Glu416
Arg418
Ala408
Gln453

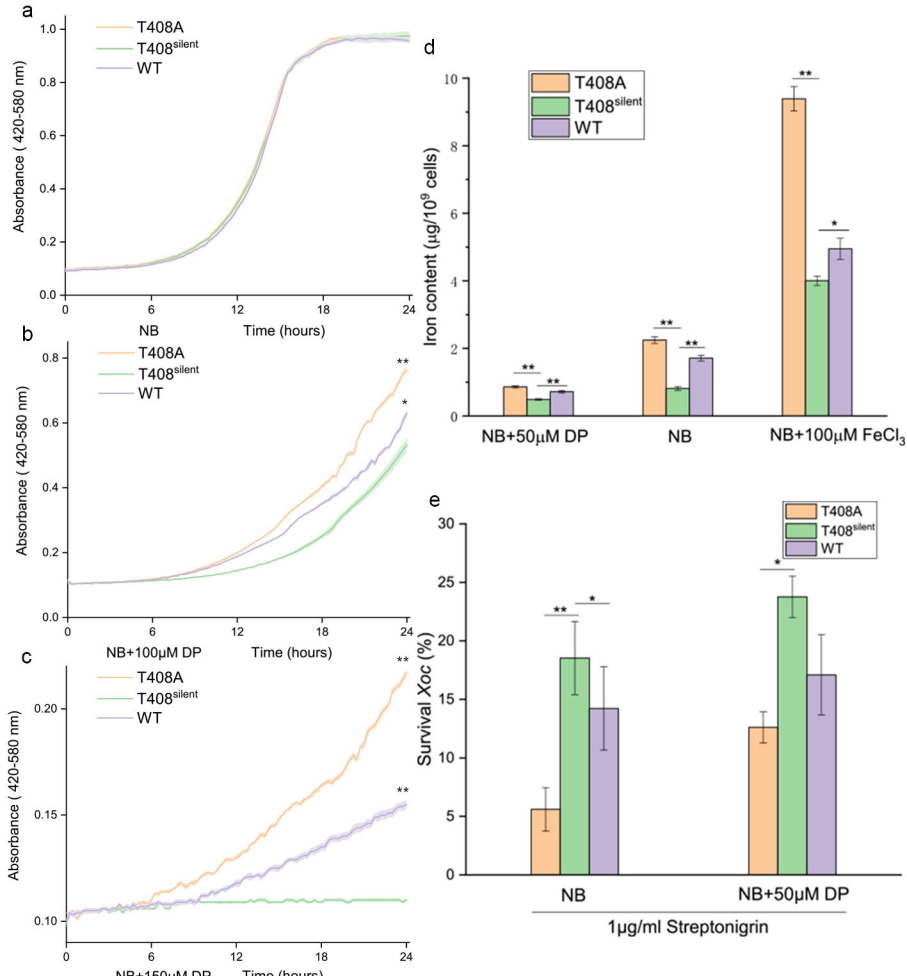
a
T408A
T408silent
WT
Absorbance (420-580 nm)
NB
Time (hours)
b
NB+100μM DP
c
NB+150μM DP
d
Iron content (μg/10^9 cells)
NB+50μM DP
NB
NB+100μM FeCl3
e
Survival Xoc (%)
1μg/ml Streptonigrin
* P < 0.05 ** P < 0.01

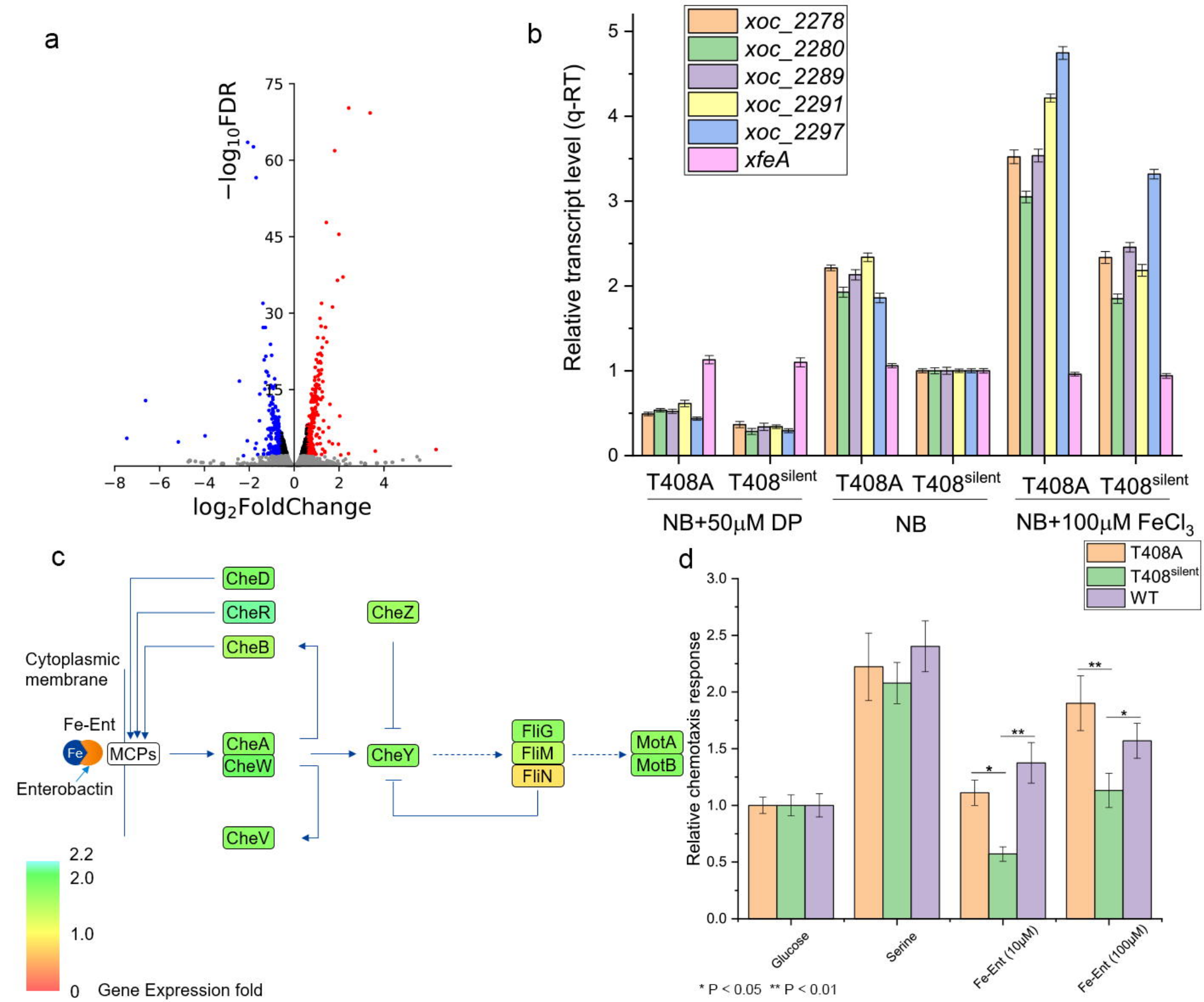
a
−log10FDR
log2FoldChange
b
Relative transcript level (q-RT)
xoc_2278
xoc_2280
xoc_2289
xoc_2291
xoc_2297
xfeA
T408A
T408silent
NB+50μM DP
NB
NB+100μM FeCl3
c
CheD
CheR
CheB
CheZ
Cytoplasmic membrane
Fe-Ent
Fe
MCPs
Enterobactin
CheA
CheW
CheY
FliG
FliM
FliN
MotA
MotB
CheV
Gene Expression fold
d
T408A
T408silent
WT
Relative chemotaxis response
Glucose
Serine
Fe-Ent (10μM)
Fe-Ent (100μM)
* P < 0.05 ** P < 0.01

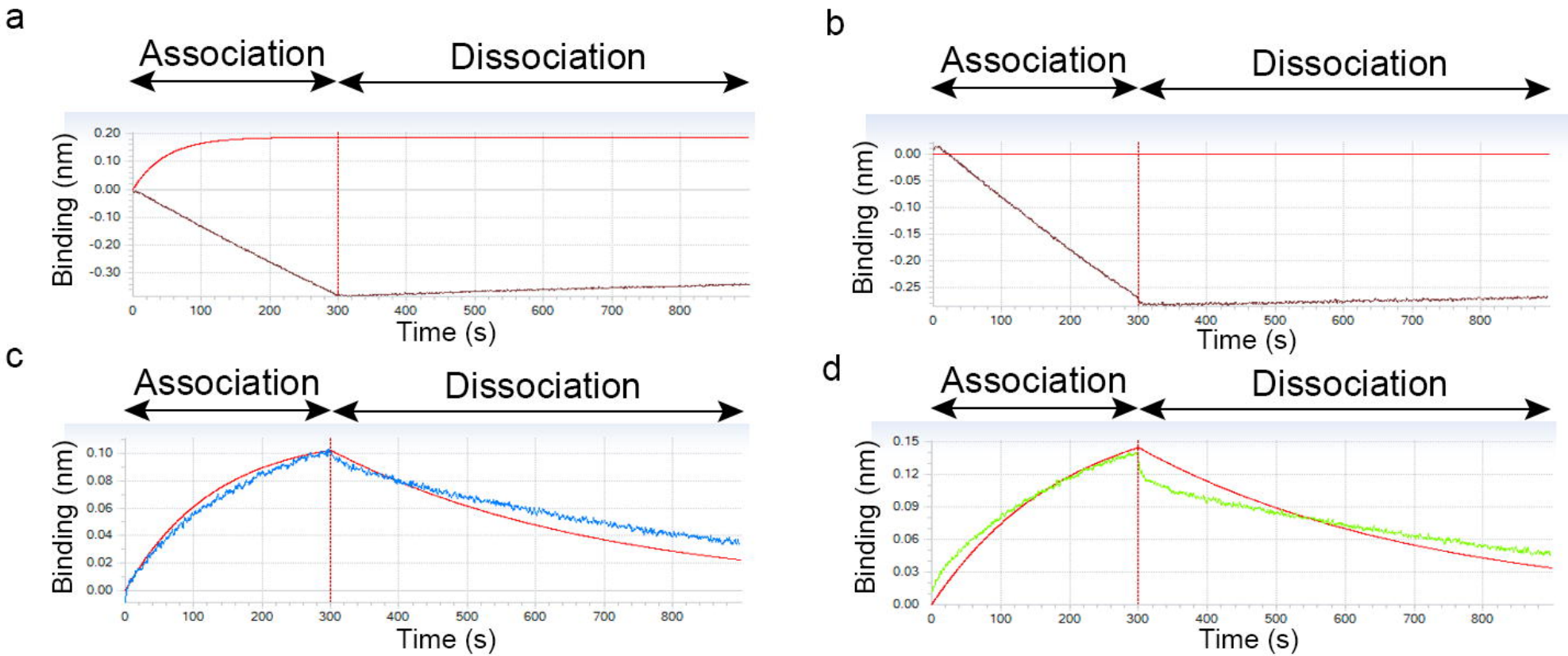
a
Association
Dissociation
Binding (nm)
0.20
0.10
0.00
-0.10
-0.20
-0.30
0
100
200
300
400
500
600
700
800
Time (s)
b
Association
Dissociation
Binding (nm)
0.00
-0.05
-0.10
-0.15
-0.20
-0.25
0
100
200
300
400
500
600
700
800
Time (s)
c
Association
Dissociation
Binding (nm)
0.10
0.08
0.06
0.04
0.02
0.00
0
100
200
300
400
500
600
700
800
Time (s)
d
Association
Dissociation
Binding (nm)
0.15
0.12
0.09
0.06
0.03
0.00
0
100
200
300
400
500
600
700
800
Time (s)

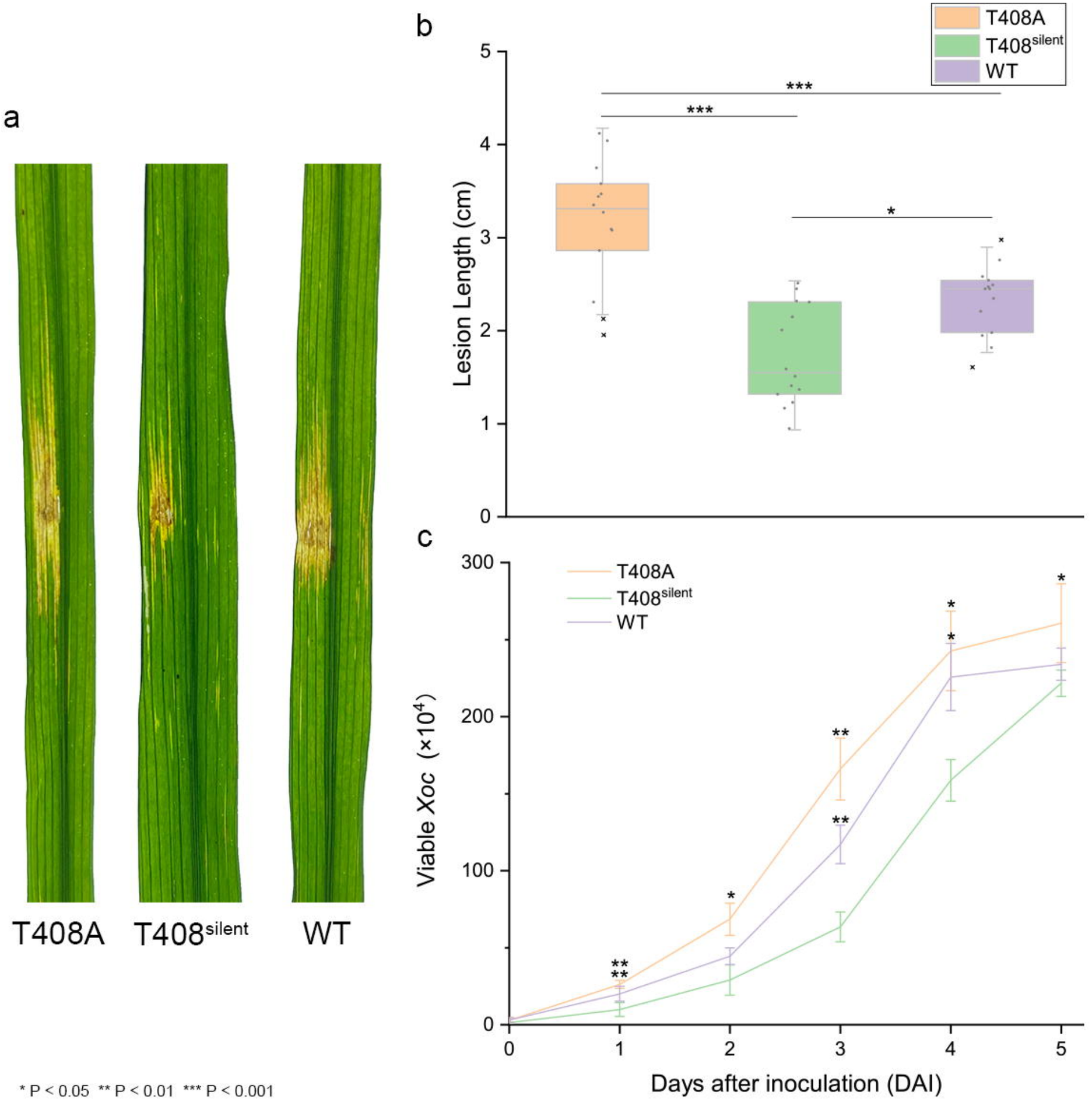
a
T408A
T408silent
WT
b
T408A
T408silent
WT
Lesion Length (cm)
0
1
2
3
4
5
***
***
*
c
T408A
T408silent
WT
Viable Xoc (×10^4)
0
100
200
300
Days after inoculation (DAI)
0
1
2
3
4
5
* P < 0.05 ** P < 0.01 *** P < 0.001

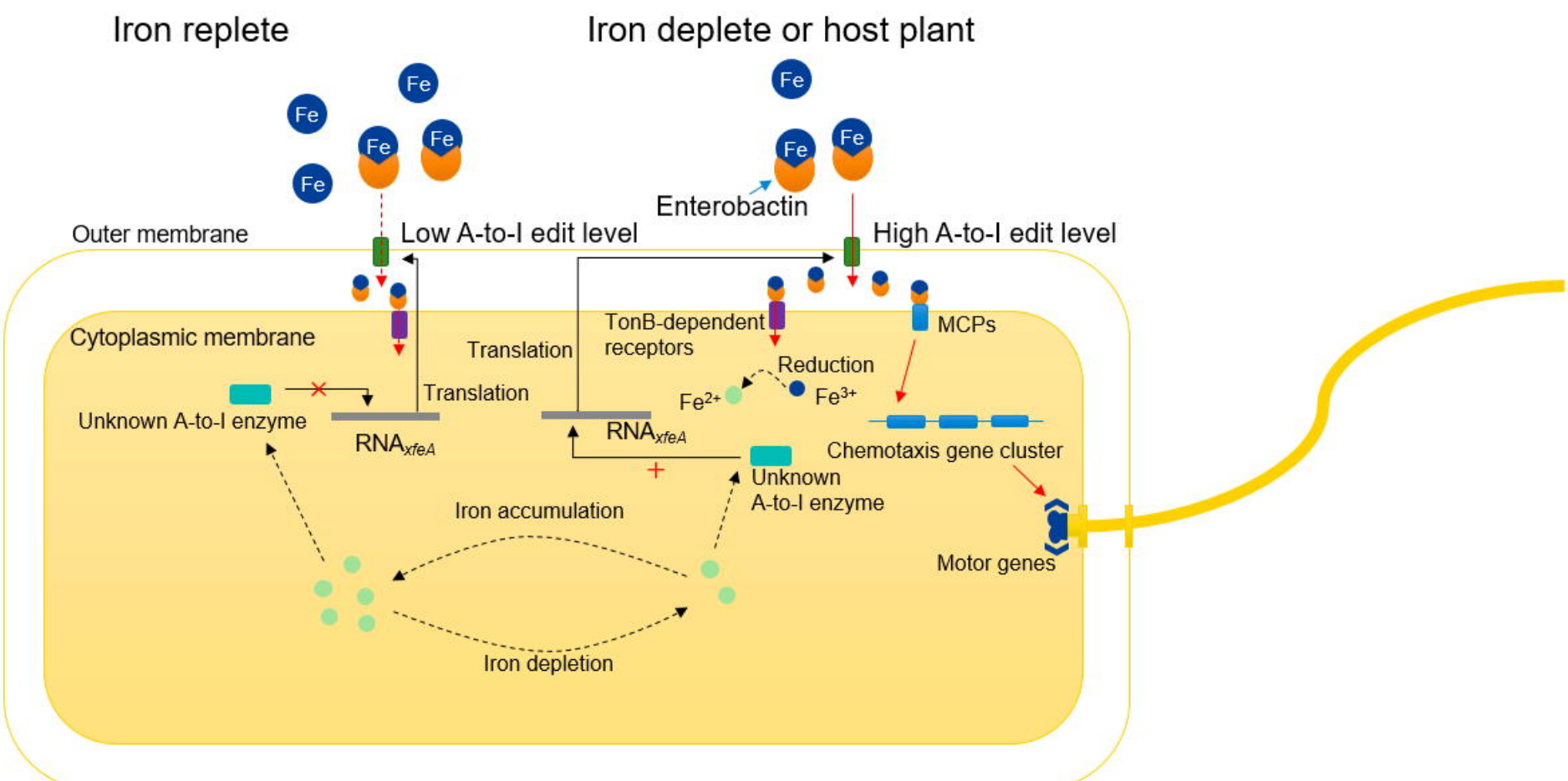
Iron replete
Iron deplete or host plant
Fe
Fe
Fe
Fe
Fe
Fe
Fe
Fe
Enterobactin
Outer membrane
Low A-to-I edit level
High A-to-I edit level
Cytoplasmic membrane
Translation
TonB-dependent receptors
MCPs
Reduction
Translation
Fe2+
Fe3+
Unknown A-to-I enzyme
RNAxfeA
RNAxfeA
Chemotaxis gene cluster
+
Unknown A-to-I enzyme
Iron accumulation
Motor genes
Iron depletion